Hindawi Publishing Corporation
Mathematical Problems in Engineering
Volume 2014, Article ID 676202, 13 pages
http://dx.doi.org/10.1155/2014/676202

Research Article

Sensorless Stator Field-Oriented Controlled IM Drive at Low Speed with R_r Estimator

Wen-Cheng Pu, Yung-Chang Luo, and Po-Yan Chu

Department of Electrical Engineering, National Chin-Yi University of Technology, Taichung 41170, Taiwan

Correspondence should be addressed to Wen-Cheng Pu; puo@ncut.edu.tw

Received 1 March 2014; Accepted 18 April 2014; Published 16 June 2014

Academic Editor: Her-Terng Yau

This paper pertains to a technique of a sensorless indirect stator field-oriented induction motor control, which prevents the accumulative errors incurred by the integrator and the problem relating to the stability of the control system caused by the stator resistance susceptible to temperature variations while conducting the flux estimation directly and computing the synchronous rotary speed. The research adds an adaptive flux observer to estimate the speed of the rotor and uses the fixed trace algorithm (FTA) to execute an online estimation of the slip difference, thereby improving the system of stability under the low rotary speed at regenerating mode and the influence of the rotor resistance on the slip angle. Finally, the paper conducts simulations by Simulink of MATLAB and practices to verify the correctness of the result the paper presents.

1. Introduction

Induction motors are broadly applied to industrial machines due to their simple configuration and easy maintenance. However, the induction motor is the nonlinear and time-varying system, so the variable-transmission drive system of the early-stage induction motor has not been easily carried out until the field-oriented control theory was developed by Blaschke in the year 1972 and the rapid development of the algorithm technique for semiconductor came to overcome these problems [1–3]. To save the space and maintain and decrease the influence of promiscuous signals of the speed sensor on the reliability and the antinoise capability of the control system of the induction motor, researches on sensorless speed controller have been claimed incessantly [4–7]. It can be classified into the flux estimation mode and the model reference adaptive mode [4]. The former conducts the estimation by using an open-loop method, so it is susceptible to variations of motor parameters. The latter adopts the structure of the model adaptive mode in order to obtain a preferable system response and accuracy of estimation [1, 8]. However, when this estimation system is operated in the low rotary speed at regenerating mode, unstable areas still exist, which would affect the sturdiness of the entire sensorless speed control system [5]. In order to operate the entire estimation system in the low rotary speed at regenerating mode, this research adds the observer and uses the Routh Stability Criterion to obtain the observer feedback gain under the stabilized system [1, 6]. Further, the stator field-oriented control configuration is relatively simple, so it is often applied to the vehicle traction control system. The system can be classified into a direct control and an indirect control. The former adopts the integration induction voltage to estimate the flux directly and compute the synchronous speed. However, the integrator accumulates errors easily, and the generation of incorrect parameters of the stator resistance affects the estimation result as well. Therefore, this research adopts the latter. The shortcoming of the latter is that the accuracy of estimating the slip difference is affected as the slip estimation is susceptible to the rotor resistance which is subjected to temperature changes, and thence the conversion of coordinates and the stability of the system are also affected. Accordingly, the subject research adopts the rotor observer by the fixed trace algorithm (FTA) to estimate the rotor resistance [2, 9].

Therefore, the subject research applies an indirect stator field-oriented structure to control the induction motor, adopts the adaptive observer to estimate the rotor speed of the motor for the demand for low rotary speed regenerating mode, and uses the fixed trace algorithm (FTA) to estimate the rotor resistance, thereby increasing the control stability and accuracy of the induction motor.

2. Methodology

2.1. Dynamic of the Induction Motor. Under the random d-q coordinate system, the electrical equations for the stator side and the rotor side of the induction motor can be, respectively, expressed by

$$\left[\left(R_s + L_s p\right)\mathbf{I} + \omega L_s \mathbf{J}\right]\overrightarrow{i_s^a} + \left[L_m p\mathbf{I} + \omega L_m \mathbf{J}\right]\overrightarrow{i_r^a} = \overrightarrow{v_s^a} \quad (1)$$

$$\begin{aligned}&\left[L_m p\mathbf{I} + L_m\left(\omega - \omega_r\right)\mathbf{J}\right]\overrightarrow{i_s^a}\\ &\quad + \left[\left(R_r + L_r p\right)\mathbf{I} + L_r\left(\omega - \omega_r\right)\mathbf{J}\right]\overrightarrow{i_r^a} = 0.\end{aligned} \quad (2)$$

Under the random coordinate, the stator flux $\overrightarrow{\phi_s^a}$ and the rotor flux $\overrightarrow{\phi_r^a}$ can be, respectively, expressed by

$$\overrightarrow{\phi_s^a} = L_s\overrightarrow{i_s^a} + L_m\overrightarrow{i_r^a}, \quad (3)$$

$$\overrightarrow{\phi_r^a} = L_m\overrightarrow{i_s^a} + L_r\overrightarrow{i_r^a}, \quad (4)$$

wherein the stator voltage is $\overrightarrow{v_s^a} = \left[v_{ds}^a \;\; v_{qs}^a\right]^T$, the stator current is $\overrightarrow{i_s^a} = \left[i_{ds}^a \;\; i_{qs}^a\right]^T$, the rotor current is $\overrightarrow{i_r^a} = \left[i_{dr}^a \;\; i_{qr}^a\right]^T$, the stator flux is $\overrightarrow{\phi_s^a} = \left[\phi_{ds}^a \;\; \phi_{qs}^a\right]^T$, the rotor flux is $\overrightarrow{\phi_r^a} = \left[\phi_{dr}^a \;\; \phi_{qr}^a\right]^T$, the motor parameters, such as R_S, R_r, L_S, L_r, and L_m are, respectively, are denoted by the stator resistance, the rotor resistance, the stator inductance, the rotor inductance, and the mutual inductance, ω and ω_r are denoted by the speed of the random angle and the speed of the rotor angle, $p = d/dt$, $\mathbf{I} = \left[\begin{smallmatrix}1 & 0\\ 0 & 1\end{smallmatrix}\right]$, and $\mathbf{J} = \left[\begin{smallmatrix}0 & -1\\ 1 & 0\end{smallmatrix}\right]$.

Formula (3) can be rewritten by $\overrightarrow{i_r^a} = (1/L_m)(\overrightarrow{\phi_r^a} - L_s\overrightarrow{i_s^a})$, then substitute it into equations (1) and (2); then convert the formula into the synchronous coordinate system ($\omega = \omega_e$), and thence get

$$R_s\mathbf{I}\overrightarrow{i_s^e} + \left(p\mathbf{I} + \omega_e\mathbf{J}\right)\overrightarrow{\phi_s^e} = \overrightarrow{v_s^e}, \quad (5)$$

$$\begin{aligned}&-\frac{L_s}{L_m}\left[\left(R_r + \sigma L_r p\right)\mathbf{I} + \sigma L_r\omega_{sl}\mathbf{J}\right]\overrightarrow{i_s^e}\\ &\quad + \frac{L_r}{L_m}\left[\left(\frac{1}{\tau_r} + p\right)\mathbf{I} + \omega_{sl}\mathbf{J}\right]\overrightarrow{\phi_s^e} = 0.\end{aligned} \quad (6)$$

Finally, formulas (5) and (6) are arranged into the dynamic as follows:

$$p\mathbf{X} = A\mathbf{X} + B\overrightarrow{v_s^e}, \quad (7)$$

$$\overrightarrow{i_s^e} = C\mathbf{X}, \quad (8)$$

wherein

$$\begin{aligned}\mathbf{X} &= \left[\overrightarrow{i_s^e} \;\; \overrightarrow{\phi_s^e}\right]^T,\\ A &= \begin{bmatrix}A_{11} & A_{12}\\ A_{21} & A_{22}\end{bmatrix},\\ B &= \left[\frac{1}{L_\sigma} \;\; 1\right]^T,\\ C &= \left[1 \;\; 0\right],\\ A_{11} &= -\left(\frac{R_s}{L_s} + \frac{1}{\tau_r\sigma}\right)\mathbf{I} - \left(\omega_e - \omega_r\right)\mathbf{J},\\ A_{12} &= \frac{1}{L_\sigma}\left(\frac{1}{\tau_r}\mathbf{I} - \omega_r\mathbf{J}\right),\\ A_{21} &= -R_s\mathbf{I},\\ A_{22} &= -\omega_e\mathbf{J},\\ \tau_r &= \frac{L_r}{R_r},\\ L_\sigma &= L_s - \frac{{L_m}^2}{L_r},\end{aligned} \quad (9)$$

and ω_e is the speed of the synchronous angle.

2.2. Full-Order Adaptive Speed Estimator. Formulas (7) and (8) are added into the full-order flux observer and arranged as

$$p\widehat{\mathbf{X}} = \widehat{A}\widehat{\mathbf{X}} + B\overrightarrow{v_s^e} + H\left(\overrightarrow{i_s^e} - \widehat{\overrightarrow{i_s^e}}\right) \quad (10)$$

$$\widehat{\overrightarrow{i_s^e}} = C\widehat{\mathbf{X}}, \quad (11)$$

wherein, the symbol "$\widehat{\ }$" represents an estimated value, $\widehat{A} = \left[\begin{smallmatrix}\widehat{A}_{11} & \widehat{A}_{12}\\ A_{21} & A_{22}\end{smallmatrix}\right]$, $\widehat{A}_{11} = -(R_s/L_s + 1/\tau_r\sigma)\mathbf{I} - (\omega_e - \widehat{\omega}_r)\mathbf{J}$, $\widehat{A}_{12} = (1/L_\sigma)((1/\tau_r)\mathbf{I} - \widehat{\omega}_r\mathbf{J})$, $H_1 = h_1\mathbf{I} + h_2\mathbf{J}$, $H_2 = h_3\mathbf{I} + h_4\mathbf{J}$, and $H = \left[\begin{smallmatrix}H_1\\ H_2\end{smallmatrix}\right]$ represents the observer feedback gain matrix.

According to the model reference adaptive system, formulas (7) and (8) are the model reference and formulas (10) and (11) are the adjustable model. To make a subtraction between formulas (7) and (10) as well as a subtraction between formulas (8) and (11), respectively, get

$$pe = Ae + \Delta A\widehat{\mathbf{X}} - H\left(\overrightarrow{i_s^e} - \widehat{\overrightarrow{i_s^e}}\right) \quad (12)$$

$$e_i = Ce, \quad (13)$$

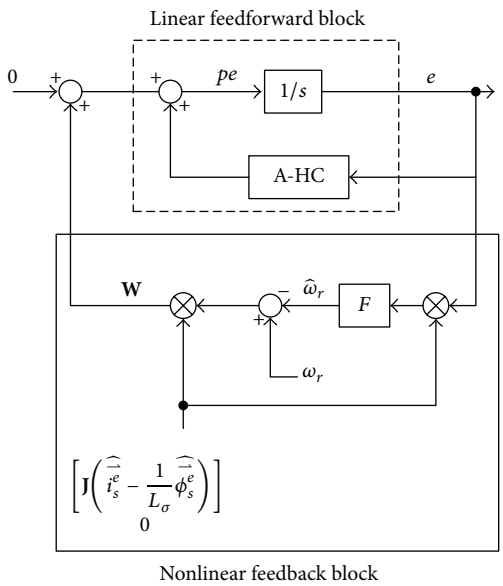

Figure 1: Model reference adaptive system block.

wherein, in formulas (12) and (13), $e = [e_i \;\; e_\phi]^T$, $e_i = \vec{i}_s^e - \hat{\vec{i}}_s^e$, $e_\phi = \vec{\phi}_s^e - \hat{\vec{\phi}}_s^e$, $\Delta A = \begin{bmatrix} \Delta A_{11} & \Delta A_{12} \\ 0 & 0 \end{bmatrix}$, $\Delta A_{11} = \mathbf{J}\Delta\omega_r$, $\Delta A_{12} = -\mathbf{J}(1/L_\sigma)\Delta\omega_r$, and $\Delta\omega_r = \omega_r - \hat{\omega}_r$.

Incorporate the current difference calculated by formula (13) into formula (12) and get the following formula after the process of linearization:

$$pe = (A - HC)\, e + \mathbf{W}, \tag{14}$$

wherein W is denoted by

$$\mathbf{W} = \begin{bmatrix} \mathbf{J}\left(\hat{\vec{i}}_s^e - \frac{1}{L_\sigma}\hat{\vec{\phi}}_s^e\right)\Delta\omega_r \\ 0 \end{bmatrix}. \tag{15}$$

The structure of the rotor speed $\hat{\omega}_r$ estimator as shown in Figure 1 includes a linear feedforward block and a nonlinear feedback block, wherein the nonlinear function F, set as the subject speed estimator, is defined by

$$\hat{\omega}_r = \left(K_{p\omega} + K_{i\omega}\int dt\right) e_i^T \mathbf{J}\left(\hat{\vec{i}}_s^e - \frac{1}{L_\sigma}\hat{\vec{\phi}}_s^e\right). \tag{16}$$

In formula (16), $K_{p\omega}$ is the proportional gain and $K_{i\omega}$ is the integration gain.

With respect to the selection of the feedback gain of the observer, formulas (7) and (10) are converted into the synchronous coordinate system ($\omega = \omega_e$) while deducing and rewriting them as

$$\begin{aligned} p\vec{i}_s^e &= A_{11}\vec{i}_s^e + A_{12}\vec{\phi}_s^e + \vec{v}_s^e \\ p\vec{\phi}_s^e &= A_{21}\vec{i}_s^e + A_{22}\vec{\phi}_s^e \end{aligned} \tag{17}$$

$$\begin{aligned} p\hat{\vec{i}}_s^e &= A_{11}\hat{\vec{i}}_s^e + A_{12}\hat{\vec{\phi}}_s^e + \vec{v}_s^e + H_1\left(\vec{i}_s^e - \hat{\vec{i}}_s^e\right) \\ p\hat{\vec{\phi}}_s^e &= A_{21}\hat{\vec{i}}_s^e + A_{22}\hat{\vec{\phi}}_s^e + H_2\left(\vec{i}_s^e - \hat{\vec{i}}_s^e\right). \end{aligned} \tag{18}$$

Subtract formula (17) from formula (18) and then get an error equation as follows:

$$\begin{aligned} [s\mathbf{I} - (A_{11} - H_1)]\, e_i &= A_{12}e_\phi + \Delta A_{11}\hat{\vec{i}}_s^e + \Delta A_{12}\hat{\vec{\phi}}_s^e \\ [s\mathbf{I} - A_{22}]\, e_\phi &= (A_{21} - H_2)\, e_i. \end{aligned} \tag{19}$$

The following formula is obtained from formula (19):

$$e_i = G(s)\,\mathbf{J}\left(\hat{\vec{i}}_s^e - \frac{1}{L_\sigma}\hat{\vec{\phi}}_s^e\right), \tag{20}$$

wherein

$$\begin{aligned} G(s) &= \begin{bmatrix} G_{11} & G_{12} \\ G_{21} & G_{22} \end{bmatrix}, \\ e_i &= [e_d \;\; e_q]^T. \end{aligned} \tag{21}$$

Under a steady state,

$$e_q = G_{22}\left(\hat{i}_{ds}^e - \frac{1}{L_\sigma}\hat{\phi}_{ds}^e\right)\Delta\omega_r. \tag{22}$$

The arranged close-loop system of the full-order adaptive speed estimator is shown in Figure 2.

3. Indirect Stator Field-Oriented Control

For conducting an indirect stator field-oriented control, it needs to compute ω_{sl} during the control because the synchronous speed (ω_e) needs to estimate rotor speed (ω_r) and the slip (ω_{sl}) together. In the synchronous d-q coordinate system, when the equation derived from the stator current and the stator flux which are set as the state variables makes the q-axis component of the stator flux reach zero to acquire the slip difference speed, and the stator flux is in accordance with d-axis of the synchronous reference coordinates frame.

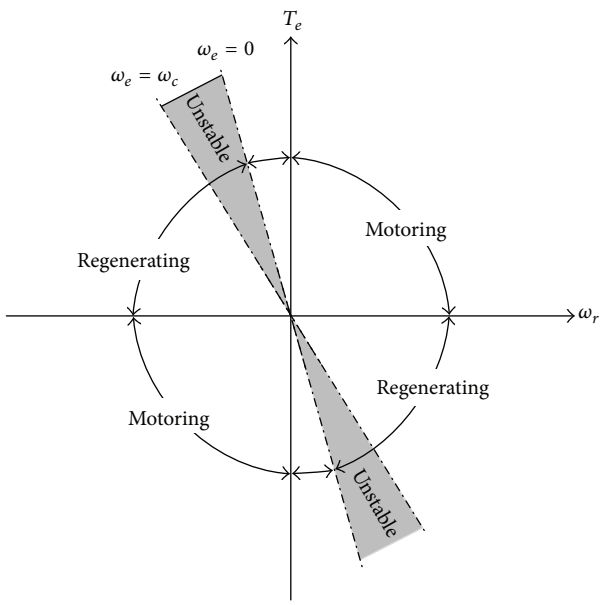

FIGURE 2: Torque-speed plane.

Hence, the slip difference speed and the d-axis stator flux can be expressed respectively, as follows:

$$\omega_{sl} = \frac{L_S\left(1+\sigma\tau_r s\right)i_{qs}^e}{\tau_r\left(\phi_{ds}^e - L_\sigma i_{ds}^e\right)}, \tag{23}$$

$$\frac{1+\tau_r s}{\left(1+\sigma\tau_r s\right)}\phi_{ds}^e = i_{ds}^e - \frac{\sigma\tau_r\omega_{sl}}{1+\sigma\tau_r s}i_{qs}^e. \tag{24}$$

In the paper, use formula (23) to estimate ω_{sl}. Furthermore, because formula (24) includes the q-axis component, the feedforward compensation quantity is added and defined by formula (25) to execute the decoupling control. Consider

$$i_{dq}^e = \frac{\sigma\tau_r\omega_{sl}}{1+\sigma\tau_r s}i_{qs}^e. \tag{25}$$

After adding the feedforward compensation quantity, formula (24) can be renewed as

$$\phi_{ds}^e = \frac{L_s\left(1+\sigma\tau_r s\right)}{1+\tau_r s}i_{qs}^e. \tag{26}$$

Herein, the electromagnetic torque T_e under the stator field-oriented control can be expressed by

$$T_e = \frac{3P}{4}i_{qs}^e\phi_{ds}^e. \tag{27}$$

And formula (5) is renewed into the following equations:

$$v_{ds}^e = R_s i_{ds}^e + p\phi_{ds}^e \tag{28}$$

$$v_{qs}^e = R_s i_{qs}^e + \omega_e\phi_{ds}^e. \tag{29}$$

As shown in formula (29), it includes the d-axis component, so the feedforward compensation quantity $\omega_e\phi_{ds}^e$ is added for subjecting the axis to the decoupling control.

4. Design of the Observer Feedback Gain

As shown in Figure 2, the transfer function G_{22} is arranged by

$$G_{22} = \frac{s^3 + xs^2 + \left(m+\omega_e^2\right)s + \omega_e\left(n+\omega_e x\right)}{\left[s^2 + xs + \left(m - \omega_e y - \omega_e^2\right)\right]^2 + \left[\left(y+2\omega_e\right)s + \left(n+\omega_e x\right)\right]^2}, \tag{30}$$

wherein

$$\begin{aligned} x &= h_1 + \frac{R_s}{L_\sigma} + \frac{1}{\sigma\tau_r} \\ y &= h_2 - \omega_r \\ m &= \frac{1}{L_\sigma}\left[\frac{1}{\tau_r}\left(R_s + h_3\right) + \omega_r h_4\right] \\ n &= \frac{1}{L_\sigma}\left[\frac{1}{\tau_r}h_4 - \omega_r\left(R_s + h_3\right)\right]. \end{aligned} \tag{31}$$

To design the observer feedback gain, the molecular equation of G_{22} is made in the Routh table as shown in (32) according to the Routh Stability Criterion. Consider

$$\begin{array}{c|cc} s^3 & 1 & m+\omega_e^2 \\ s^2 & x & n\omega_e + x\omega_e^2 \\ s^1 & \dfrac{mx - n\omega_e}{x} & 0 \\ s & n\omega_e + x\omega_e^2 & 0. \end{array} \tag{32}$$

According to the Routh table, a steady-state condition can be made as follows:

$$\begin{aligned} x &> 0 \\ mx &> n\omega_e \\ x\omega_e\left(\omega_e - \omega_c\right) &> 0 \end{aligned} \tag{33}$$

wherein

$$\omega_c = -\frac{n}{x}. \tag{34}$$

To analyse the unstable-speed area clearly, the torque-speed chart is applied to present the relationship between the two elements. As shown in formula (23), under the steady state, the slip ω_{sl} can be arranged by

$$\omega_{sl} = \frac{L_\sigma i_{qs}^e}{\phi_{ds}^e - L_\sigma i_{ds}^e}. \tag{35}$$

From formula (35),

$$i_{qs}^e = \omega_{sl}\left(\frac{\phi_{ds}^e}{L_\sigma} - i_{ds}^e\right). \tag{36}$$

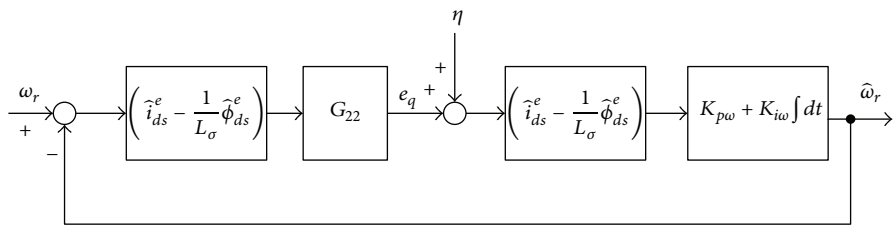

Figure 3: Close-loop system of the full-order adaptive speed estimator.

Incorporate formula (36) into formula (27) and get

$$T_e = \frac{3P}{4}\left(\frac{\phi_{ds}^{e\ 2}}{L_\sigma} - i_{ds}^e\phi_{ds}^e\right)\omega_{sl} = K_T\omega_{sl}. \tag{37}$$

In formula (37), the slip $\omega_{sl} = \omega_e - \hat{\omega}_r$ and K_T is a torque constant, which is presented by

$$K_T = \frac{3P}{4}\left(\frac{\phi_{ds}^{e\ 2}}{L_\sigma} - i_{ds}^e\phi_{ds}^e\right). \tag{38}$$

If the condition of $\omega_c = \omega_e$ is satisfied, the incorporation of formula (33) can get

$$\omega_e = \frac{R_s + h_3}{L_\sigma x}\hat{\omega}_r - \frac{h_4}{\tau_r L_\sigma x}. \tag{39}$$

Finally, incorporate formula (39) into formula (37) and arrange it; the equation is got from the torque and the rotation speed as follows:

$$T_e = a\hat{\omega}_r + b. \tag{40}$$

In formula (40), a and b are shown as follows:

$$\begin{aligned} a &= K_T\left(\frac{R_s + h_3}{L_\sigma x} - 1\right). \\ b &= -K_T\frac{h_4}{\tau_r L_\sigma x}. \end{aligned} \tag{41}$$

Figure 2 shows the torque-speed chart, wherein the x-axis represents the rotor speed of the motor ω_r and the y-axis represents the motor torque T_e. In the figure, the gray part shows that, when the speed estimator is operated in the regenerating area, an unstable part will be generated during the speed estimation, and the steady-state condition of formula (33) is used to design the observer gain to reduce the unstable part.

From the above analysis, when $\omega_c = 0$, the observer gain is

$$\begin{aligned} h_1 &= -\left(\frac{R_s}{L_\sigma} + \frac{1}{\sigma\tau_r}\right) + k, \\ h_2 &= k\omega_r, \\ h_3 &= 0, \\ h_4 &= \tau_r R_s\omega_r, \\ k &> 0, \end{aligned} \tag{42}$$

wherein, to satisfy the steady-state condition, a positive integer k larger than zero is selected and the observer feedback gain $h_1 \sim h_4$ incorporates with x, y, m, and n, respectively, to get

$$\begin{aligned} x &= k, \\ y &= (k-1)\,\omega_r, \\ m &= \frac{1}{L_\sigma}\left[\frac{R_s}{\tau_r} + \omega_r^2\tau_r R_s\right], \\ n &= 0. \end{aligned} \tag{43}$$

5. Design of PI Gain Parameters of the Speed Estimator

In the single-input single-output close-loop system of Figure 3, η represents the noise which affects the speed estimation, and the paper inferred from the influence of the noise that

$$\frac{\hat{\omega}}{\eta} = \frac{\left(\hat{i}_{ds}^e - (1/L_\sigma)\,\hat{\phi}_{ds}^e\right)\left(K_{p\omega} + K_{i\omega}/s\right)}{1 + G_{22}\left(\hat{i}_{ds}^e - (1/L_\sigma)\hat{\phi}_{ds}^e\right)^2\left(K_{p\omega} + K_{i\omega}/s\right)}. \tag{44}$$

To consider the influence of the high frequency noise on the speed estimation, incorporate $s = j\infty$ into formula (44) and infer that

$$\left.\frac{\hat{\omega}}{\eta}\right|_{s=j\infty} = \left(\hat{i}_{ds}^e - \frac{1}{L_\sigma}\hat{\phi}_{ds}^e\right)K_{p\omega}. \tag{45}$$

From formula (45), it can be found that the size of the proportional gain $K_{p\omega}$ can restrict the high frequency noise, so the proportional gain $K_{p\omega}$ selected smaller value to reduce the influence of the noise on the speed estimator. Considering the effect of the low frequency noise, it can incorporate $s = j0$ into formula (44) and arrange it to get

$$\left.\frac{\hat{\omega}}{\eta}\right|_{s=j0} = \frac{1}{\left(\hat{i}_{ds}^e - (1/L_\sigma)\hat{\phi}_{ds}^e\right)G_{22}\big|_{s=j0}}. \tag{46}$$

From formula (46), the adjustment to the proportional gain $K_{p\omega}$ or the integration gain $K_{I\omega}$ cannot improve the influence of the low frequency noise on the speed estimator. However, consider the influence of the proportional and integration gain of the motor acceleration/deceleration on the speed estimator (R can be set as an acceleration/deceleration velocity) and infer from formula (47) that a selection of

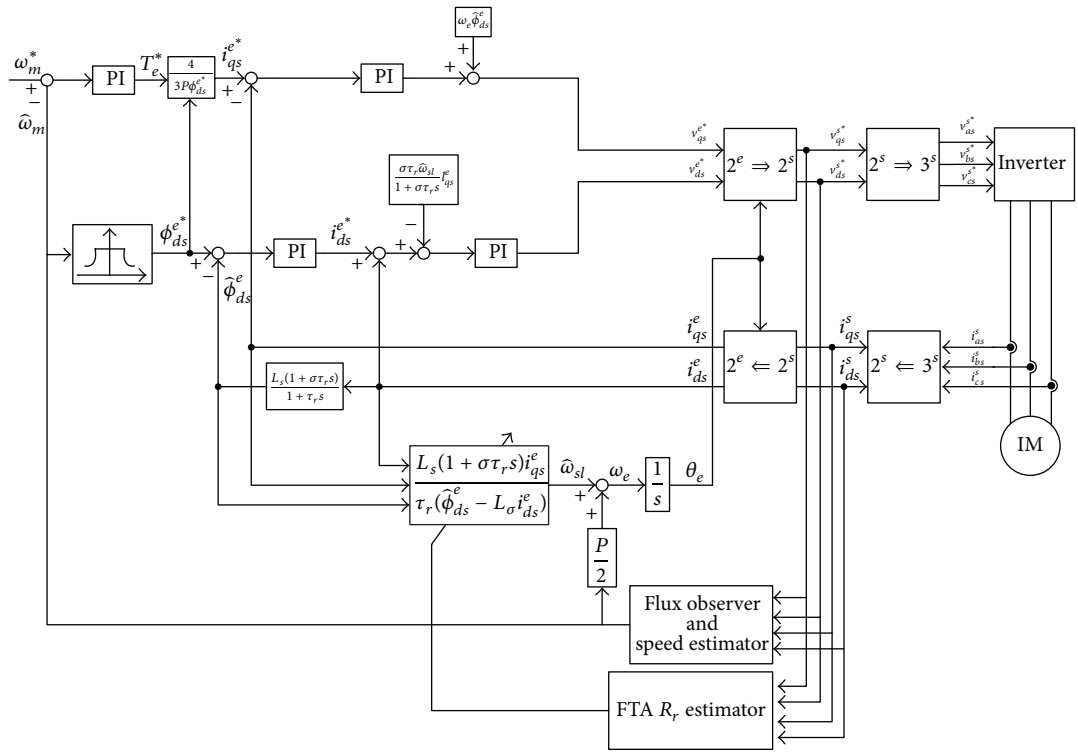

Figure 4: Integral block of speed sensorless controller.

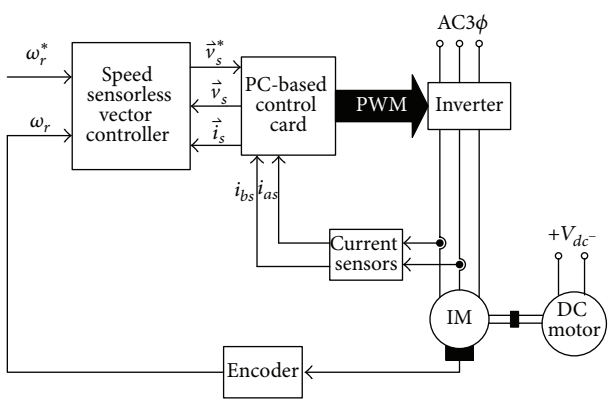

Figure 5: The structure of the experimental platform.

Table 1

Maximum output power	1 HP
Phase	3
Rated voltage	220 V
Rated current	3.1 A
Rated rotary speed	1680 rpm
P (pole)	4
R_s	2.85 Ω
R_r	2.3433 Ω
L_s	0.1967 H
L_r	0.1967 H
L_m	0.1886 H
J_m	$0.009\ \mathrm{N \cdot m \cdot sec^2/rad}$
B_m	$0.00825\ \mathrm{N \cdot m \cdot sec^2/rad}$

the value of the integration gain $K_{I\omega}$ can affect the steady-state error of the speed estimation as the error e_s is set by acceleration/deceleration during a slope input speed. When the integration result is increased, the steady-state error of the speed is relatively decreased to increase the accuracy of the speed estimator. Consider

$$e_s = \lim_{s\to 0} s \times \frac{R}{s^2} \times \frac{1}{1 + G_{22}\left(\widehat{i}^e_{ds} - (1/L_\sigma)\widehat{\phi}^e_{ds}\right)^2 \left(K_{p\omega} + K_{i\omega}/s\right)}$$
$$= \frac{R}{K_{i\omega}\left(\widehat{i}^e_{ds} - (1/L_\sigma)\,\widehat{\phi}^e_{ds}\right)^2 G_{22}\Big|_{s=0}}. \tag{47}$$

6. Estimation of Rotor Resistance by FTA

Rewrite formula (3) as $\overrightarrow{i^s_s} = (1/L_m)(\overrightarrow{\phi^s_r} - L_r\overrightarrow{i^s_r})$ and incorporate formula (2) to get

$$p\phi^s_{dr} = -R_r i^s_{dr} - \omega_r \phi^s_{qr} \tag{48}$$

$$p\phi^s_{qr} = -R_r i^s_{qr} - \omega_r \phi^s_{dr}. \tag{49}$$

Then rewrite formula (49) as

$$\omega_r = \frac{p\phi^s_{qr} + R_r i^s_{qr}}{\phi^s_{dr}}. \tag{50}$$

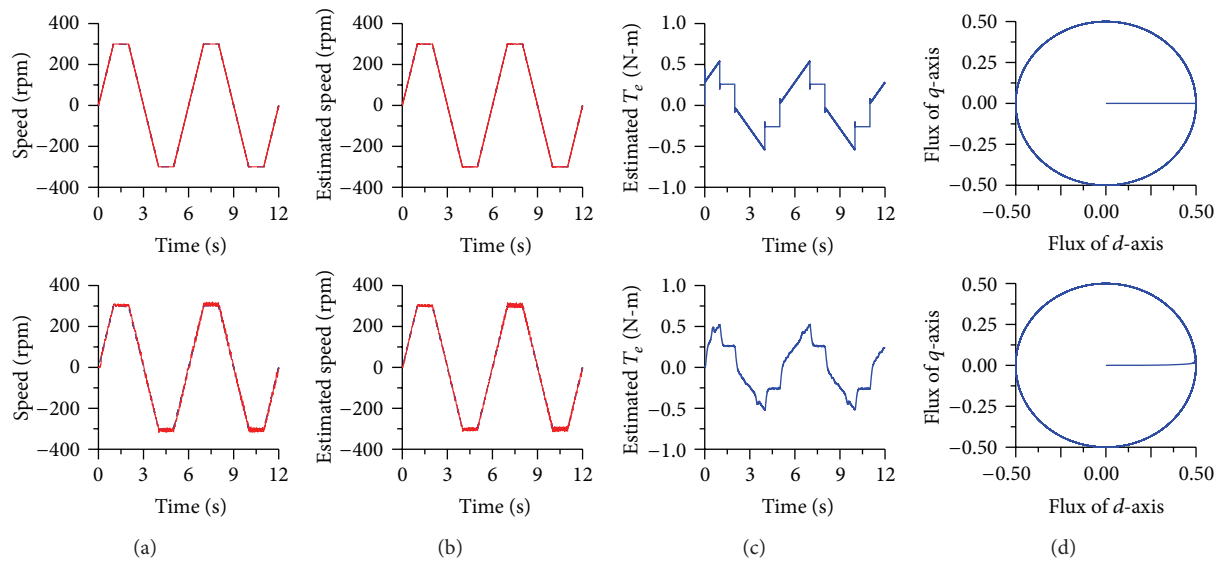

FIGURE 6: Simulation and Practical data of the induction motor at 300 rpm. (a) Actual motor speed. (b) Estimated motor speed. (c) Stator flux. (d) Estimated torque.

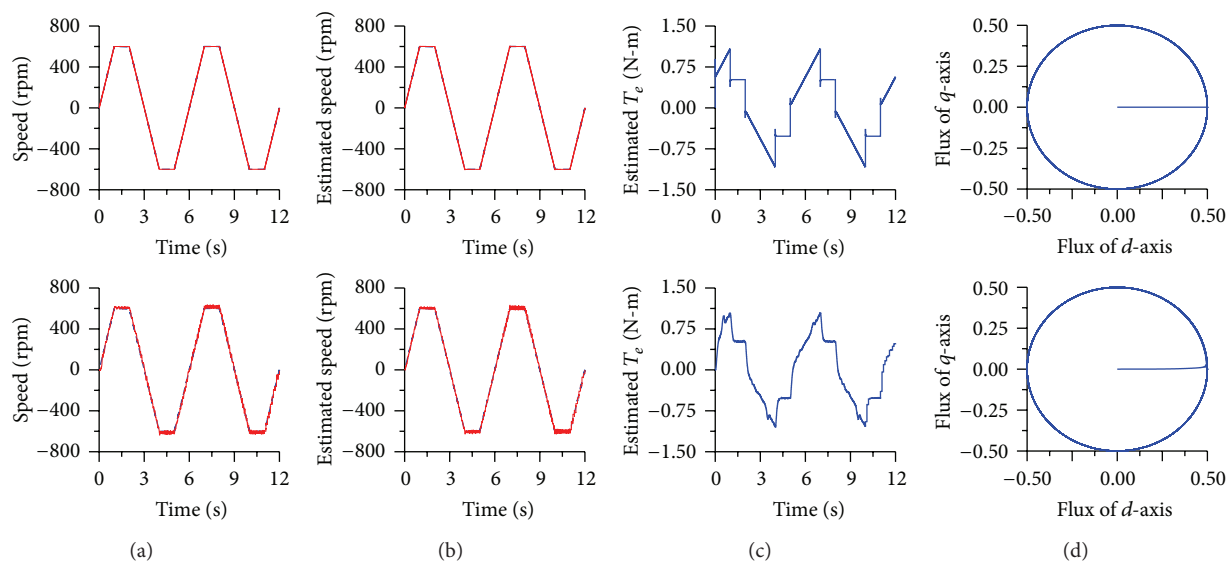

FIGURE 7: Simulation and Practical data of the induction motor at 600 rpm. (a) Actual motor speed. (b) Estimated motor speed. (c) Stator flux. (d) Estimated torque.

Incorporate formula (50) into formula (48) and arrange it to get the formula of the estimated rotor resistance R_r and thence rewrite it according to the fixed trace algorithm (FTA) as follows:

$$R_r = -\frac{p\phi_{dr}^s\phi_{dr}^s + p\phi_{qr}^s\phi_{qr}^s}{i_{dr}^s\phi_{dr}^s + i_{qr}^s\phi_{qr}^s} \tag{51}$$

or

$$\widehat{R}_r[n] = \widehat{R}r[n-1] - \frac{ra[n]}{1 + r(a[n])^2}\left(\widehat{R}_r[n-1]\,a[n] - b[n]\right), \tag{52}$$

wherein $a[n] = -(i_{dr}^s\phi_{dr}^s + i_{qr}^s\phi_{qr}^s)$, $b[n] = p\phi_{dr}^s\phi_{dr}^s + p\phi_{qr}^s\phi_{qr}^s$, and r represents the gain. This paper adopts the estimated rotor resistance R_r of this formula.

7. Results of Simulation and Experiment

To verify the feasibility and sturdiness of the subject system, an experimental platformas shown in Figure 5 is constituted. According to the structure of the system shown in Figure 4, it executed simulations and experiments by controlling different situations. First, the personal computer of Simulink

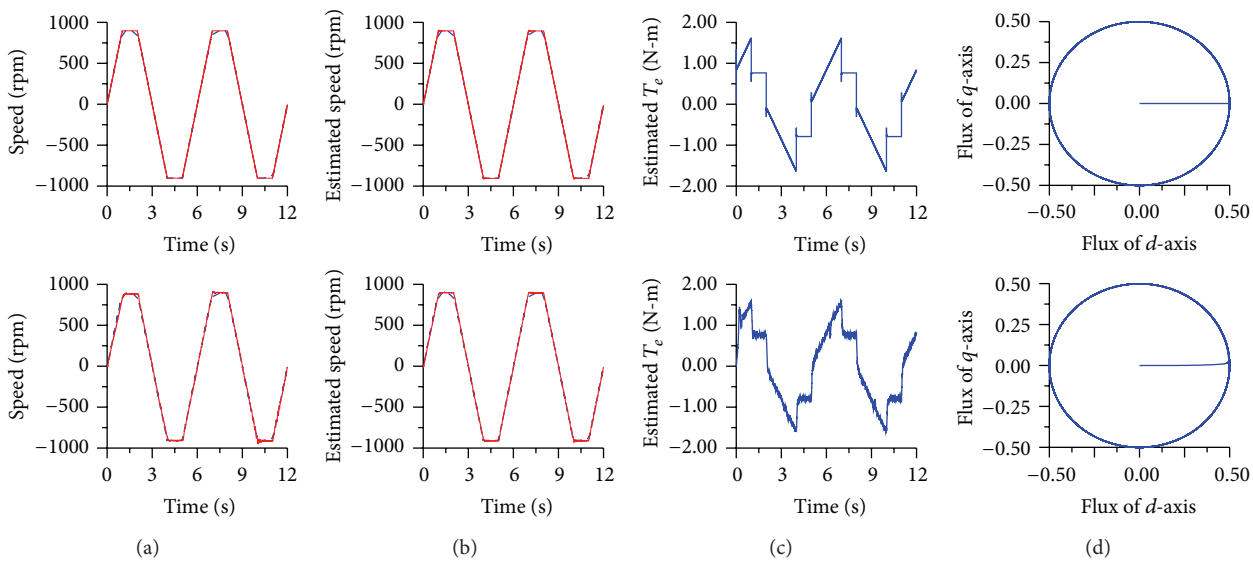

Figure 8: Simulation and Practical data of the induction motor at 900 rpm. (a) Actual motor speed. (b) Estimated motor speed. (c) Stator flux. (d) Estimated torque.

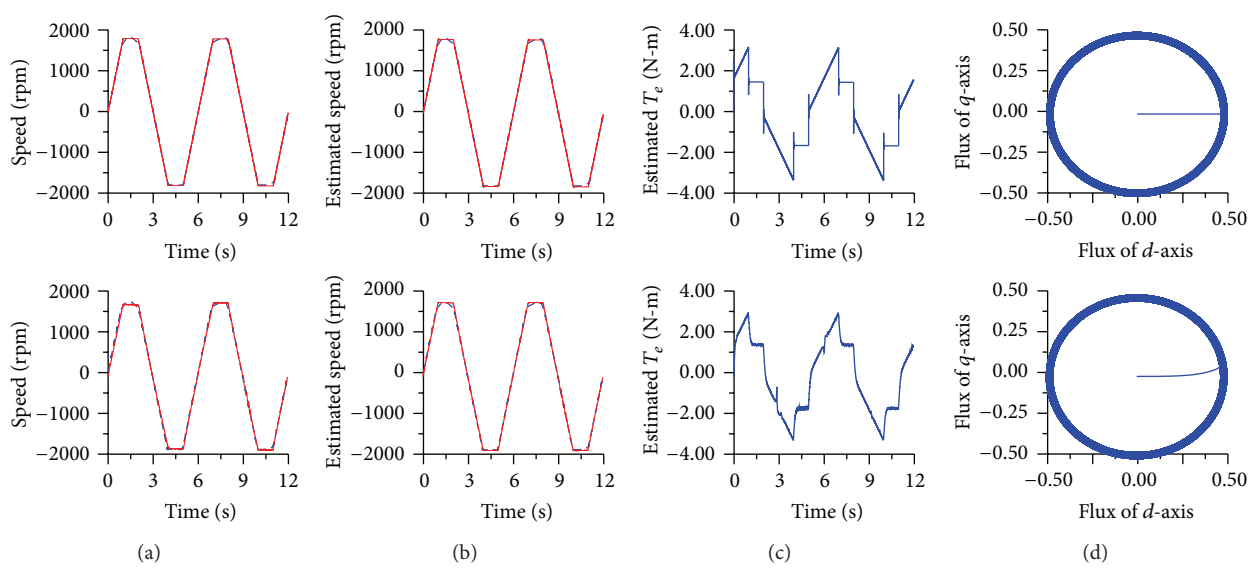

Figure 9: Simulation and Practical data of the induction motor at 1800 rpm. (a) Actual motor speed. (b) Estimated motor speed. (c) Stator flux. (d) Estimated torque.

program containing MATLAB is the speed sensorless vector controller, which functions as the simulation process. The result of the simulation drives the induction motor via PC-based control card which controls the inverter practically. The specification of the induction motor is shown in Table 1. During the experiment, there are three different rotor speeds, namely, ±1800 rpm, ±900 rpm, ±600 rpm, and ±300 rpm, and conduct the simulation of controlling the acceleration and deceleration under the nonloading and loading modes. Results are shown in Figures 6, 7, 8, and 9. Figures 10, 11, 12, and 13, respectively, show the simulation results while loading 1 N-m under the rotor speed of the induction motor commanded at ±300 rpm, ±900 rpm, ±600 rpm, and ±1800 rpm. Figures 6–9, respectively, show the nonloading practical data when the induction motor is at ±300 rpm, ±900 rpm, and ±1800 rpm. Figures 10–13, respectively, show the practical data of loading 1 N-m under the rotor speed of the induction motor commanded at ±300 rpm, ±900 rpm, and ±1800 rpm.

As shown from Figures 6–13, the upper part shows the simulation result and the lower part shows the experimental result, wherein (a) and (b) represent the respective comparisons between the simulations and experiments of

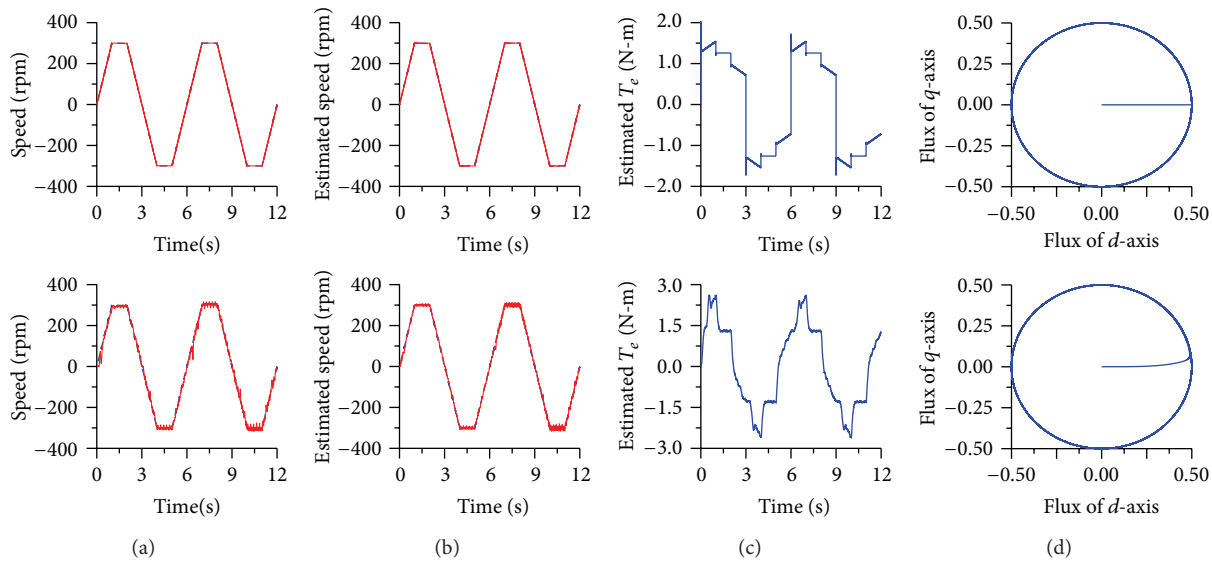

Figure 10: Loading simulation and Practical data of the induction motor at 300 rpm. (a) Actual motor speed. (b) Estimated motor speed. (c) Stator flux. (d) Estimated torque.

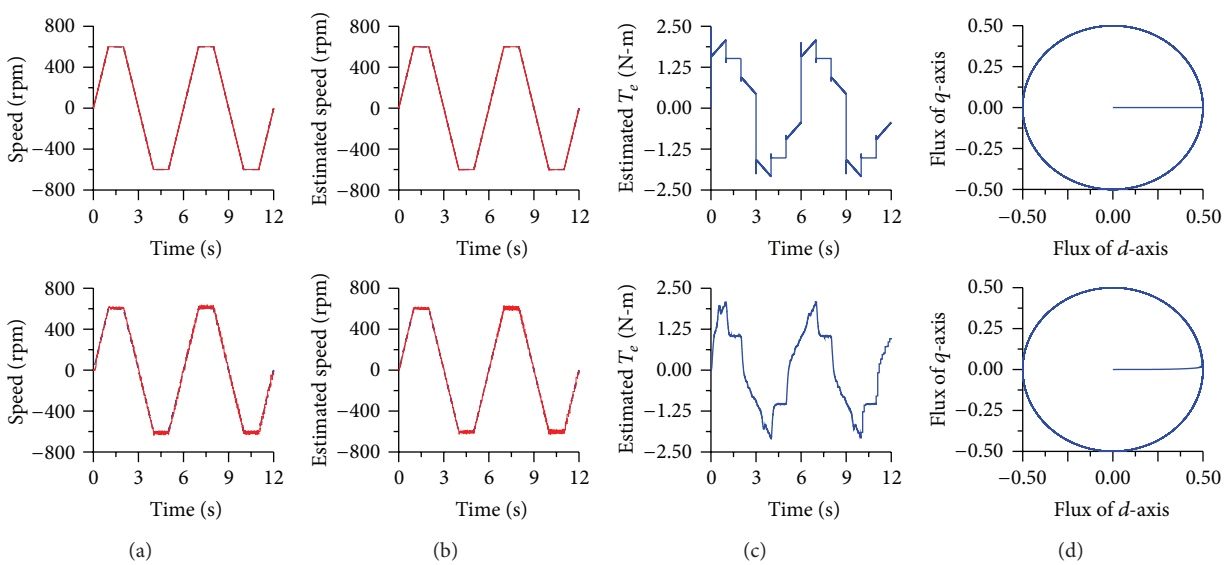

Figure 11: Loading simulation and Practical data of the induction motor at 600 rpm. (a) Actual motor speed. (b) Estimated motor speed. (c) Stator flux. (d) Estimated torque.

the actual and estimated motor speed. The x-axis shows the time with the unit showing the seconds (sec) and the y-axis shows the rotor speed with the unit showing the speed per minute (rpm). The blue solid line represents the speed command, wherein 0-1 seconds can be the clockwise acceleration of the motor, 1-2 seconds can be the constant and clockwise rotation of the motor, 2-3 seconds can be the clockwise deceleration of the motor, 3-4 seconds can be the counterclockwise acceleration, 4-5 seconds can be the constant and counterclockwise rotation of the motor, and 5-6 seconds can be the counterclockwise deceleration of the motor. (c) is the motor estimated torque, wherein the x-axis shows the time with the unit showing the seconds (sec) and y-axis shows the motor torque with the unit showing the Newton meter (N-m). (d) is the stator flux circle, wherein the x-axis shows the stator flux of d-axis component and y-axis shows the stator flux of q-axis component.

From Figures 6–9 showing the results of simulations and experiments of the motor in the nonloading clockwise and counterclockwise rotations, Figure 17 can verify that, when the motor is operated at the acceleration/deceleration speed, the estimator can estimate the actual rotation speed of the motor accurately and catch the commanded speed of the motor rapidly. When the motor is operated at the constant

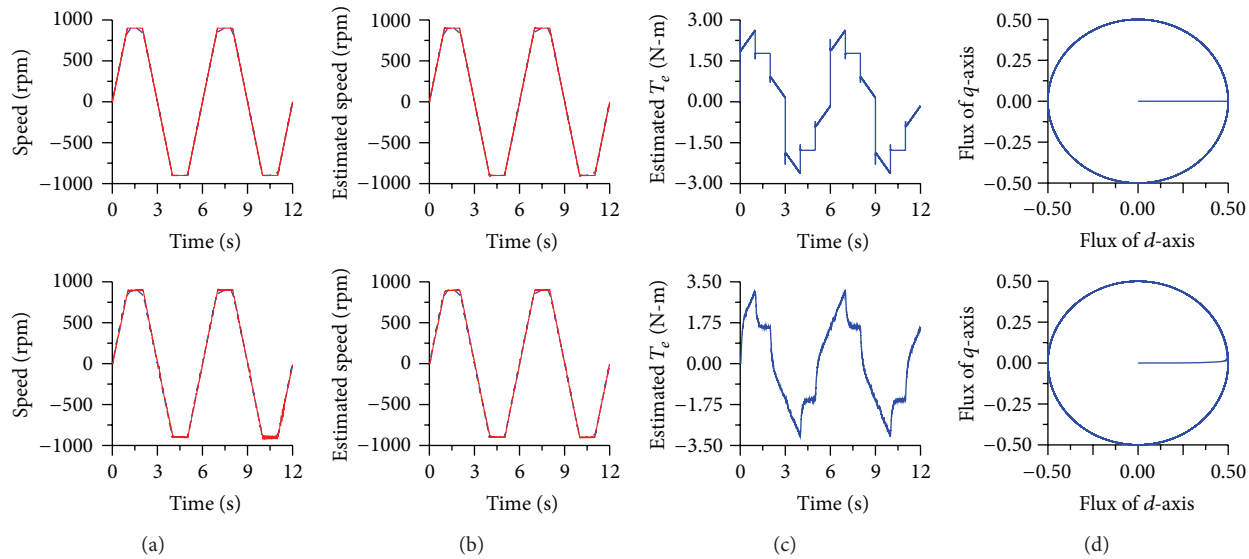

Figure 12: Loading simulation and Practical data of the induction motor at 900 rpm. (a) Actual motor speed. (b) Estimated motor speed. (c) Stator flux. (d) Estimated torque.

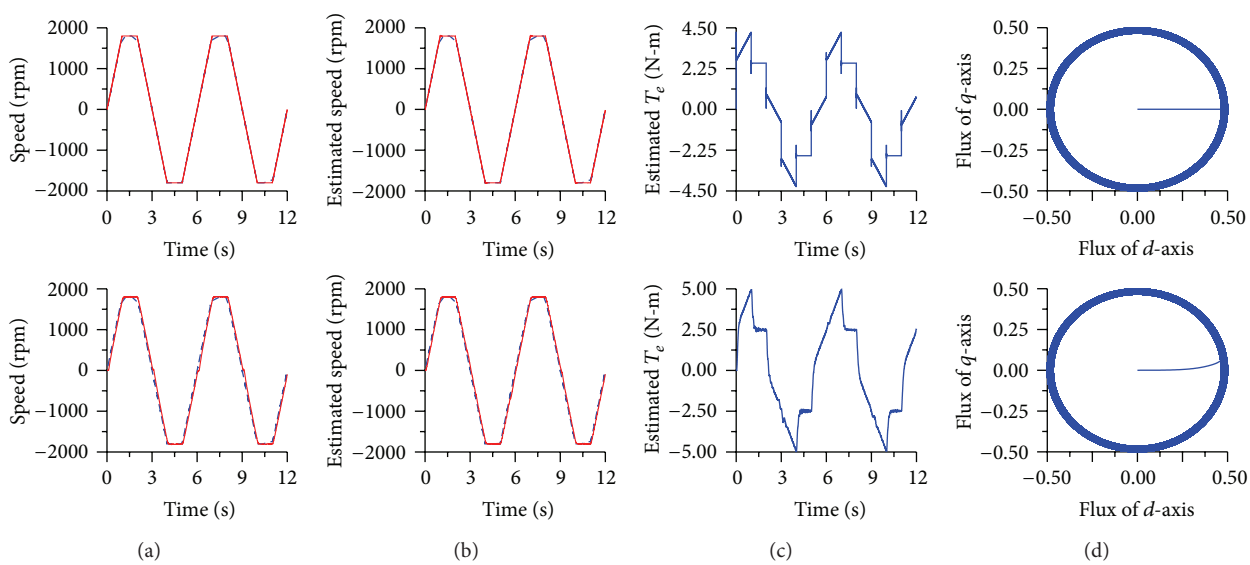

Figure 13: Loading simulation and Practical data of the induction motor at 1800 rpm. (a) Actual motor speed. (b) Estimated motor speed. (c) Stator flux. (d) Estimated torque.

speed, the estimator can estimate the actual rotation speed of the motor accurately and render the motor able to follow the commanded speed stably. In Figures 10–13, when the motor is loaded by 1 N-m, the estimator can also estimate the actual speed accurately and catch the commanded speed rapidly. The simulations and experiments shown in Figures 6–13 can verify that the speed estimator can possess a wide-range speed estimation regardless of the loading or nonloading condition.

Furthermore, for the operation under the low rotary speed regenerating test, Figure 14 and Figure 15 show respective data derived from simulating and practicing when the rotor speed to be set at 100 rpm and loading −1 N-m at the 3rd second, wherein Figure 14(a) is the simulation data without adding the observer feedback gain. Figure 14(b) is the simulation data with the addition of the observer feedback gain. Figure 15(a) is the practical data without adding the observer feedback gain. Figure 15(b) is the practical data with the addition of the observer feedback gain. From the data in Figures 14 and 15, when the verification controller is operated in the low rotary speed regenerating mode, it can select the adequate observer feedback gain and estimate the rotor speed correctly and steadily. As shown in Figure 16(a), if the rotor resistance is raised by 30% in 2-3 seconds due to the increased temperature, the estimation result of FTA

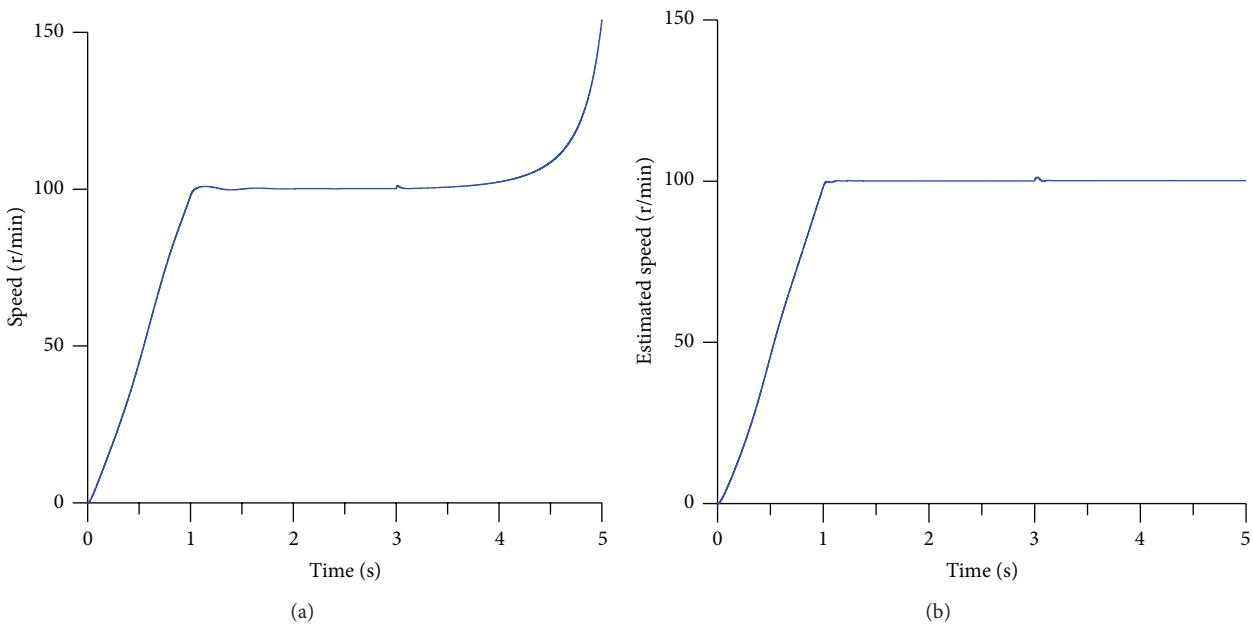

Figure 14: Simulation data of the speed estimation under the regenerating mode of the rotor speed at 100 rpm. (a) Without adding feedback gain. (b) Adding feedback gain.

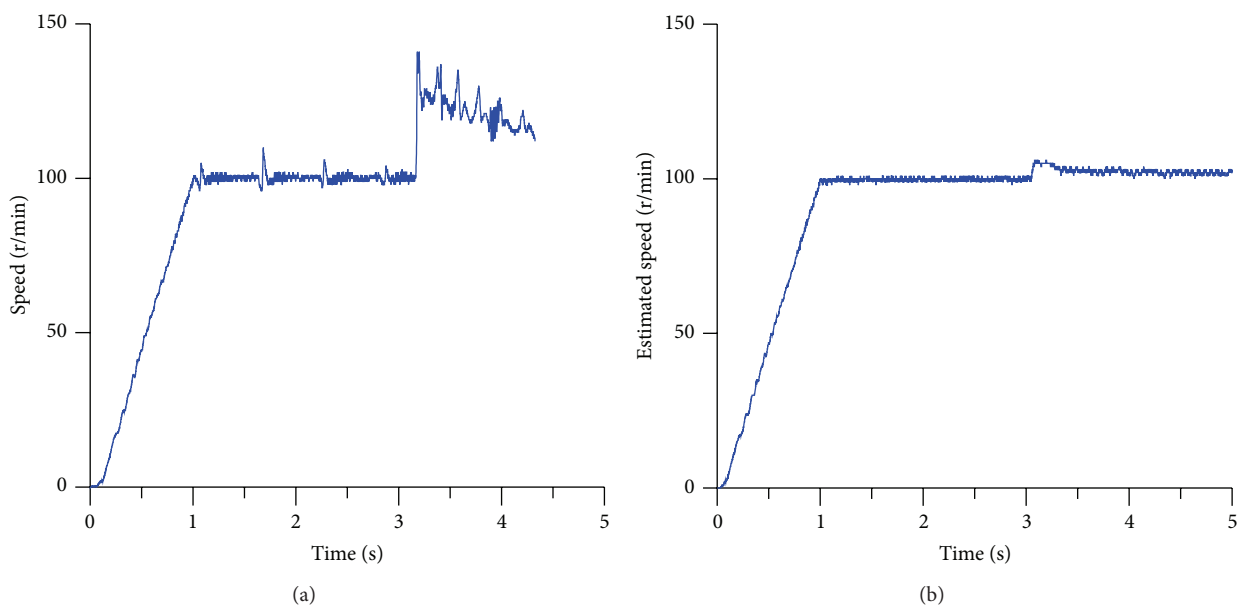

Figure 15: Practical data of the speed estimation under the regenerating mode of the rotor speed at 100 rpm. (a) Without adding feedback gain. (b) Adding feedback gain.

to the rotor resistance is shown in the figure. The dotted line in the figure denotes the actual value of the rotor resistance of the motor, and the solid line in the figure denotes the estimated value of the rotor resistance giving the slip angle. When the rotor resistance estimator is not added, the generation of error on the synchronous angle can be read in Figure 16(b), wherein the dotted line denotes the reference value of the synchronous angle and the solid line denotes the estimated value of the synchronous angle. Figure 17 shows the data after adding the rotor resistance estimator, from which the synchronous angle can be accurately estimated. Figure 18 shows the estimation results of the simulation and experiment of the rotor resistance by the fixed trace algorithm (FTA), from which it can verify that FTA can estimate the rotor resistance accurately. Figure 19 shows that the result of simulation without FTA when actual rotor resistance is

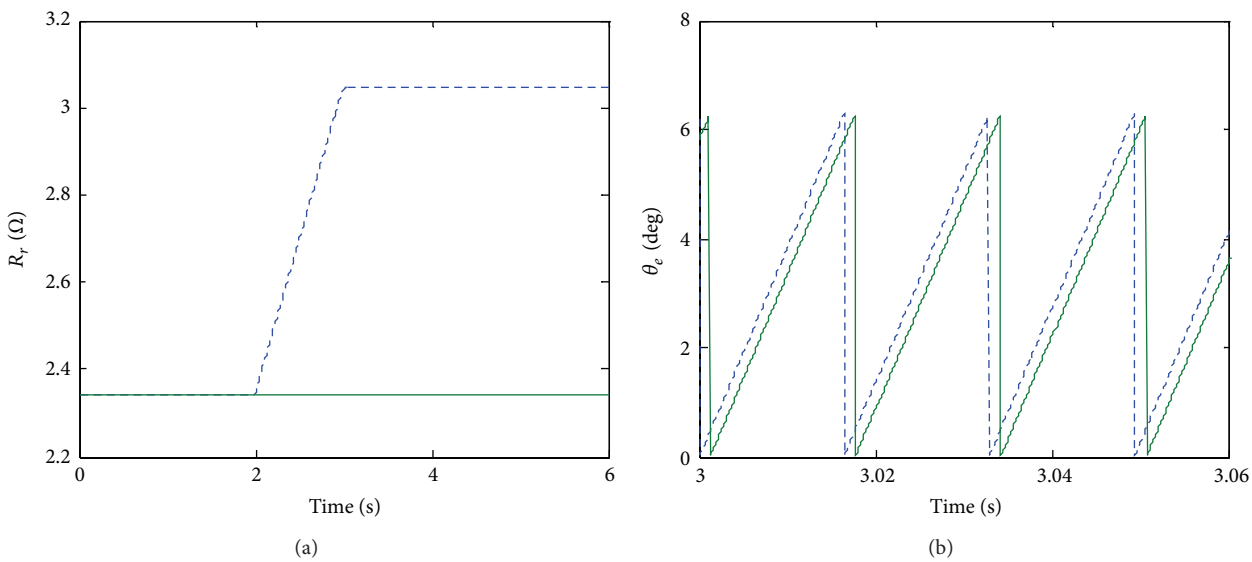

Figure 16: Estimation result of synchronous angle θ_e without adding the rotor resistance estimator under variations of R_r. (a) Rotor resistance. (b) Synchronous angle.

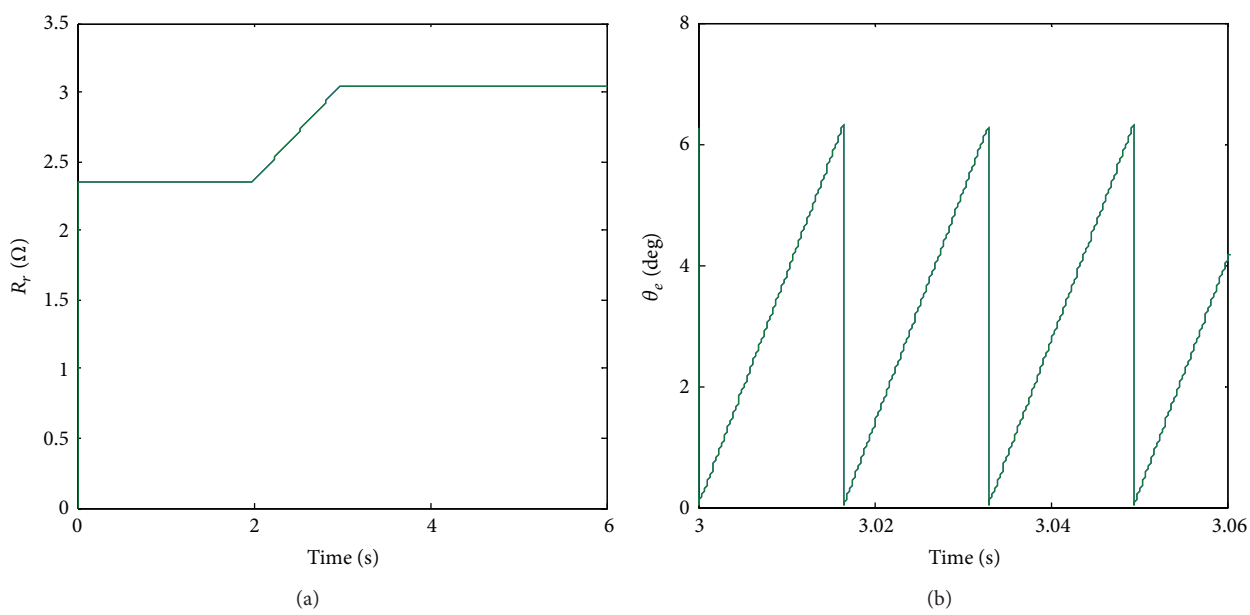

Figure 17: Estimation result of synchronous angle θ_e by adding the rotor resistance estimator under variations of R_r. (a) Rotor resistance. (b) Synchronous angle.

changed caused by temperature variations. It is unstable and it verifies the feasibility and sturdiness of the method set forth in the research.

8. Conclusion

The subject sensorless indirect stator field-oriented control technique provides a set of standard designed steps to be operated under the low rotary speed at regenerating mode and the circumstance of the unstable system. This paper further considers that the property of changes of the rotor resistance caused by variations of temperature would affect the accuracy of estimating the synchronous angle, so this paper combines the FTA which conducts the online and instant estimation of the rotor resistance in order to solve the problem of incorrect estimation of the synchronous angle incurred by the changes of the rotor resistance. Finally, the simulation and practical results can verify the feasibility and sturdiness of the method set forth in the research.

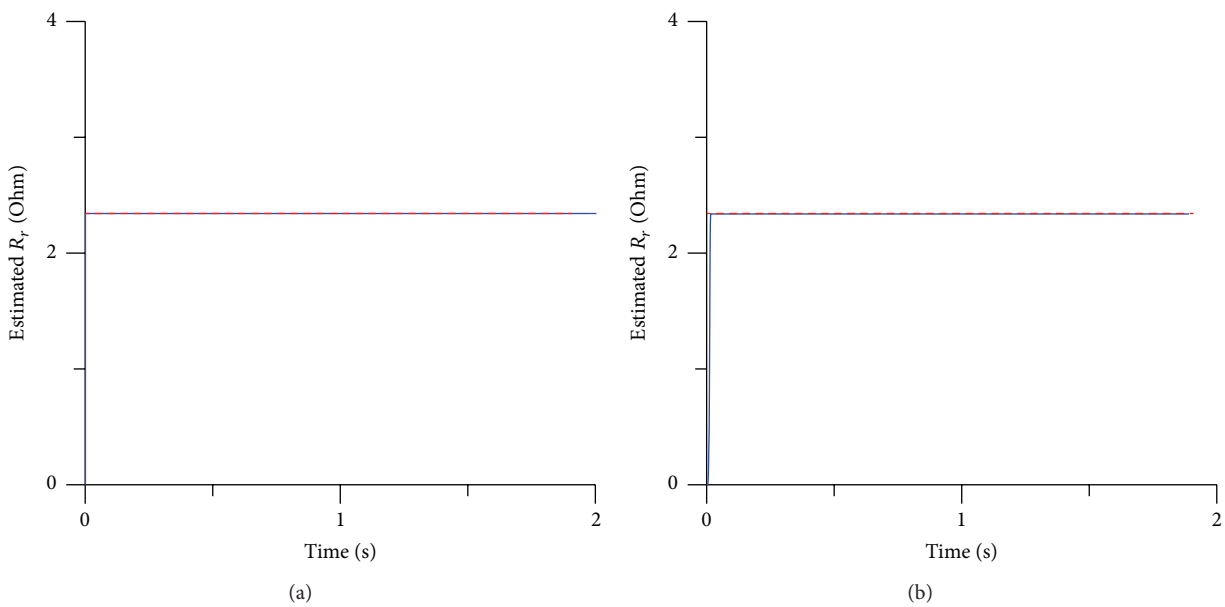

Figure 18: Results of simulation and experimental of the rotor resistance estimator by FTA. (a) Simulation results, (b) Experimental results.

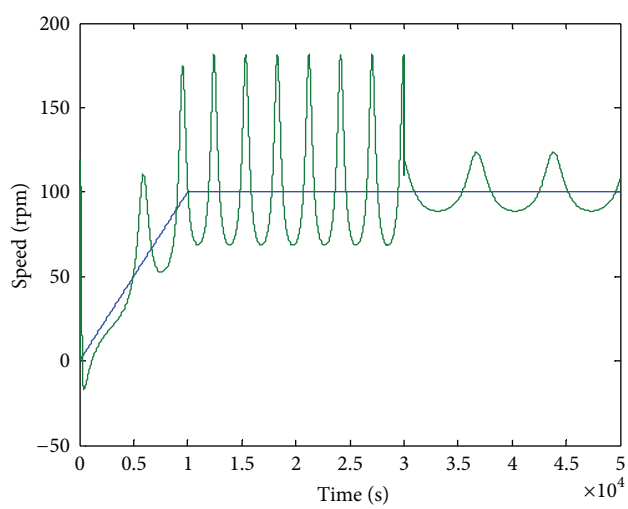

Figure 19: Results of simulation without FTA when actual rotor resistance is changed disagree with controller parameter.

Conflict of Interests

The authors declare that there is no conflict of interests regarding the publication of this paper.

References

[1] W.-C. Pu and C.-H. Liu, "Stabilization of regenerating mode at low speeds for adaptive speed sensorless induction motor drives," *Journal of the Chinese Institute of Electrical Engineering*, vol. 33, no. 2, pp. 229–242, 2010.

[2] Y.-C. Luo and C.-C. Lin, "Fuzzy MRAS based speed estimation for sensorless stator field oriented controlled induction motor drive," in *Proceedings of the International Symposium on Computer, Communication, Control and Automation (3CA '10)*, pp. 152–155, May 2010.

[3] F. Blaschke, "The principle of field orientation applies to the new transvector close-loop control system for rotating field machines," *Siemens Review*, vol. 39, no. 5, pp. 217–220, 1972.

[4] J. Holtz, "Sensorless control of induction motor drives," *Proceedings of the IEEE*, vol. 90, no. 8, pp. 1359–1394, 2002.

[5] S. Suwankawin and S. Sangwongwanich, "A speed-sensorless IM drive with decoupling control and stability analysis of speed estimation," *IEEE Transactions on Industrial Electronics*, vol. 49, no. 2, pp. 444–455, 2002.

[6] S. Suwankawin and S. Sangwongwanich, "Design strategy of an adaptive full-order observer for speed-sensorless induction-motor drives—tracking performance and stabilization," *IEEE Transactions on Industrial Electronics*, vol. 53, no. 1, pp. 96–119, 2006.

[7] M. S. Zaky, "Stability analysis of speed and stator resistance estimators for sensorless induction motor drives," *IEEE Transactions on Industrial Electronics*, vol. 59, no. 2, pp. 858–870, 2012.

[8] C. Schauder, "Adaptive speed identification for vector control of induction motors without rotational transducers," *IEEE Transactions on Industry Applications*, vol. 28, no. 5, pp. 1054–1061, 1992.

[9] Y.-C. Lo, C.-P. Hung, and C.-K. Lai, "Sensorless direct torque control drive with the online adaptive capability to stator and rotor resistances of the induction motor," *Journal of National Chin-Yi University of Technology*, vol. 21, no. 1, 2003.